Appendix for: 'Constrained deep neural network architecture search for IoT devices accounting hardware calibration'

Anonymous Author(s)
Affiliation
Address
email

The following Sections cover technical details of our work. Section 1 defines the search spaces and manually designed sampling laws, Section 2 provides statistics over networks sampled from the defined laws, Section 3 details data augmentation and hyper-parameters used for training and Section 4 justifies the choice of the IoT device and explains the workflow to export a model from the back-end framework and to deploy it on the IoT device. Section 5 elaborates how we scale our algorithm to multiple datasets and provides further information of the datasets.

1 Search space and sampling law definition

Table 1: Search spaces induced from established reference models

Space	Reference model	Params	Ops	Our Acc[1]	Ref Acc[2] [5]
S_1	DenseNet121 [13]	7.0M	898.1M	94.13%	95.04%
S_2	MobileNetV2 [12]	2.3M	94.6M	92.94%	94.43%
S_3	GoogLeNet [20]	6.2M	1.5G	93.55%	-
S_4	PNASNetA [15]	135.5K	29.2M	83.85%	-
S_5	ResNeXt29_32x4d [22]	4.8M	779.6M	93.46%	94.73%

[1] reproduced results with our training limited to 100 epochs
[2] reference results of third-party implementation with high-effort training of 350 epochs

Table 1 lists the five search spaces used in this work that are based on established models. Typical models consist of 2M up to 7M of parameters and cause workloads from 94.6 million up to 1.5 billion FLOPs and are too large for fast implementations on a targeted IoT device. DenseNets [13] exists in common variants, 121, 161, 169, and 201 and we used the smallest variant (DenseNet121) as starting point. We reproduced the accuracy for all architectures by running our training procedure as detailed in Section 3 where we used an upper limit of 100 epochs and compare it with the claimed reference accuracy from the source from where we obtained the architecture implementation in PyTorch [3]. The latter values are slightly higher but they are obtained with a high effort training that runs for a fixed amount of 350 epochs. Additionally, the later source does not state the mean and variance of the training process neither is it completely clear if the values are obtained in a one-shot training or if the best values have been selected after repeating the training process several times. In contrast, we decided to follow a pragmatic but efficient approach of evaluating each architecture only once and to limit training effort to an affordable value of 100 epochs. This decision is motivated by the fact that we want the same training procedure to be applied to over 3'000 models. Training evaluations with high-effort would cause 3.5× more computational costs and repeating experiments to deliver statistics would at least require a repetition factor of 5×. Both aspects together cause a 17.5× increase in computation cost. In our opinion, if we are willing to pay such an increase, it would be more interesting to use an affordable approach and invest the additional budget into investigating more architectures. The increased effort would allow investigating over 50'000 network architectures. Next, we define the sampling laws and parameters used to manually enforce smaller variants of networks within the defined spaces.

DenseNets [13] consists of four stages, each repeating DenseNet unique blocks. We identified the stage-specific number of repetitions, the growth rate and the reduction factor as relevant hyper-parameters that we modify. Table 2 specifies the sampling laws. In this case, we decided to clip the repetition factor at 32 which additionally includes the configuration of DenseNet161. The normalized reduction factor is sampled with a step size of 0.01.

Table 2: Architecture search space definition S_1 with different sampling laws for DenseNets

Law	Cardinality	Densenet parameters		
		$n_i, i \in \{1,2,3,4\}$	g^*	r^{**}
L_0	$3.3 * 10^9$	$[1,32]$	$[1-32]$	$[0.0,1.0]$
L_1	$2.0 * 10^6$	$[1,8]$	$[1-8]$	$[0.2,0.8]$
L_2	$6.3 * 10^7$	$[1,16]$	$[1-16]$	$[0.2,0.8]$
L_3	$1.0 * 10^9$	$[1,32]$	$[1-32]$	$[0.5,0.8]$

* g is the growth rate, ** r is the reduction rate

MobileNetsV2 [12] consists of seven stages, each repeating MobileNetsV2 unique blocks. Each block is configured with four parameters, input number of channels, output number of channels, expansion factor, and a stride factor. To generate valid configurations, we define the first input channel number separately, since the subsequent input shape follows directly from the previous block configuration. Additionally, we restrict the stride factor per stage to either be one or two and we further require to sample exactly three twos and four ones. The reason for this choice is due to the stride parameter directly influences the spatial shape of tensors and the limitation ensures fixed downsampling over three steps from 32×32 to 4×4. Additionally, the existing intermediate last convolutional layer is separately parametrized and is used as in the original reference model as a transition layer between the last block and the final linear classifier. Table 3 states the sampling law definitions.

Table 3: Architecture search space definition S_2 with different sampling laws for MobileNets

Law	Cardinality	MobileNet parameters, $i \in [1,7]$					
		f_{in}	e_i	f_i	n_i	s_i	f_{out}
L_0	$5.2 * 10^{34}$	$[1,128]$	$[1,8]$	$[1,256]$	$[1,4]$	$[1,2]$	$[1,1280]$
L_1	$3.6 * 10^{33}$	$[16,128]$	$[1,6]$	$[16,256]$	$[1,4]$	$[1,2]$	$[128,1280]$
L_2	$2.0 * 10^{28}$	$[16,64]$	$[1,4]$	$[16,128]$	$[1,3]$	$[1,2]$	$[128,512]$
L_3	$3.1 * 10^{21}$	$[16,32]$	$[1,2]$	$[16,64]$	$[1,2]$	$[1,2]$	$[128,256]$
L_4	$4.0 * 10^{19}$	$[16,32]$	$[1,2]$	$[4,32]$	$[1,2]$	$[1,2]$	$[64,128]$
L_5	$1.4 * 10^{15}$	$[16,32]$	$[1,2]$	$[2,8]$	$[1,2]$	$[1,2]$	$[16,64]$
L_6	$4.3 * 10^{13}$	$[4,8]$	$[1,2]$	$[2,8]$	$[1,2]$	$[1,2]$	$[12,16]$

GoogLeNet [20] is composed of the characteristic Inception module, which is defined through seven intermediate channel depths. The full network is grouped into three stages, first a convolutional pre-layer, second, and third a max-pooling separates sequences that are built from two, five, and two Inception modules. Table 4 defines the sampling laws. We choose parameter specific upper bounds oriented on the reference implementation.

PNASNet-A [15] consists of three stages that are build by repeating cell-A type of blocks. The stages are separated by downsampling layers that are implemented as cell instances with a stride of two. Table 6 defines the sampling laws that affect the number of block repetitions and the number of channels used in the block, where f_2 and f_3 are relatively defined to the output shape of previous stages.

Table 4: Architecture search space definition S_3 with different sampling laws for GoogLeNetd

Law	Cardinality	GoogLeNet parameters, $i \in [1,9]$						
		f_0^0	f_i^1	f_i^2	f_i^3	f_i^4	f_i^5	f_i^6
L_0	$3.4 * 10^{122}$	$[16,256]$	$[16,384]$	$[16,192]$	$[16,384]$	$[16,48]$	$[16,128]$	$[16,128]$
L_1	$2.8 * 10^{119}$	$[16,256]$	$[16,384]$	$[16,192]$	$[16,384]$	$[16,48]$	$[16,128]$	$[16,128]$
L_2	$1.1 * 10^{97}$	$[16,256]$	$[16,64]$	$[16,64]$	$[16,64]$	$[16,32]$	$[16,32]$	$[16,32]$
L_3	$9.8 * 10^{51}$	$[16,256]$	$[16,32]$	$[8,16]$	$[16,32]$	$[4,8]$	$[4,8]$	$[4,8]$
L_4	$6.3 * 10^{39}$	$[16,128]$	$[4,8]$	$[4,8]$	$[4,8]$	$[4,8]$	$[4,8]$	$[4,8]$
L_5	$5.2 * 10^{26}$	$[8,16]$	$[4,6]$	$[4,6]$	$[4,6]$	$[4,6]$	$[4,6]$	$[4,6]$
L_6	$5.0 * 10^{38}$	$[8,16]$	$[2,6]$	$[2,6]$	$[2,6]$	$[2,6]$	$[2,6]$	$[2,6]$

$f_{i+1}^0 := f_i^1 + f_i^3 + f_i^5 + f_i^6$ for $i \geq 0$, recursive definition such that next input shape matches the previous output shape

Table 5: Architecture search space definition S_4 with different sampling laws for PNASNet-A

Law	Cardinality	PNASNet-A parameters, $i \in \{1,2,3\}$			
		n_i	f_1	d_2	d_3
L_0	$3.5 * 10^6$	$[1,12]$	$[1,128]$	$[1,4]$	$[1,4]$
L_1	$3.1 * 10^6$	$[1,12]$	$[16,128]$	$[1,4]$	$[1,4]$
L_2	$2.3 * 10^5$	$[1,8]$	$[16,64]$	$[1,3]$	$[1,3]$
L_3	$9.7 * 10^2$	$[1,3]$	$[8,16]$	$[1,2]$	$[1,2]$

Set $f_2 := f_1 * d_2$ and $f_3 := f_2 * d_3$.

ResNeXt [22] is the improvement over the typical ResNet [11] structure. It consists of a three-stage architecture where each stage repeats the bottleneck block n_i times, for $i \in \{1,2,3\}$. The block consists of the typical residual connection and follows a bottleneck design where grouped convolutions are used to reduce the kernel size. We define in the search space with the bottleneck base width f_i and the cardinality c_i. However, the total channel size that is invoked during the grouped convolution operation is of width $f_i * c_i$. Since we want to limit the product $f_i * c_i$ but we also require it to be devisable by either f_i and c_i we decided to randomly sample the later and restrict the cardinality upper bound to be l_{high}/f_i, where l_{high} denotes the upper product limit and f_i is dependent on the current sampling of the base depth. Table 6 summaries the defined random laws.

Table 6: Architecture search space definition S_5 with different sampling laws for ResNeXt

Law	Cardinality	ResNeXt parameters, $i \in [1,3]$		
		n_i	f_i	c_i
L_0	$9.5 * 10^{14}$	$[1,3]$	$[1,64]$	$[1,512]$
L_1	$2.1 * 10^{10}$	$[1,3]$	$[4,64]$	$[1,512/f_i]$
L_2	$2.4 * 10^8$	$[1,3]$	$[4,32]$	$[1,128/f_i]$
L_3	$1.5 * 10^5$	$[1,2]$	$[4,8]$	$[1,32/f_i]$

2 Statistical results of used networks

For the defined search spaces and sampling laws, we collected statistics over 1000 networks that are presented in Figure 1. We targeted to cover the full domain in $[10^3, 10^7]$. Some search spaces, such as S_1, S_3, and S_5 are quickly covered with three simple configurations. Other search spaces, such as S_2 and S_3, lead to narrower distributions. We decided to add three additional sampling laws to cover the lower domain. The right-hand side of Figure 1 shows statistics obtained when networks

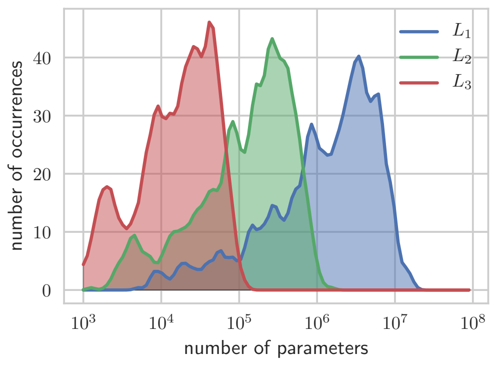

(a) Manual laws on S_1

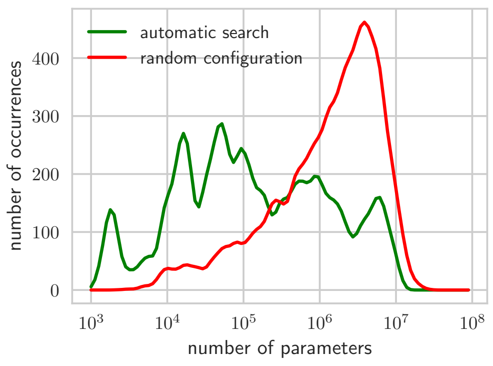

(b) Automatic law on S_1

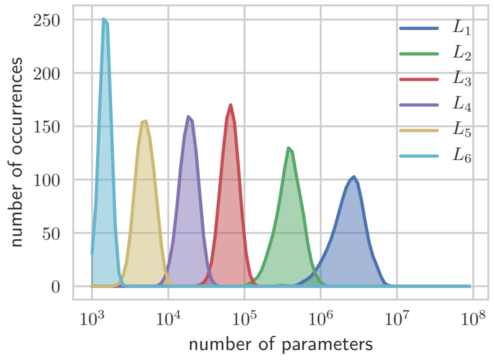

(c) Manual laws on S_2

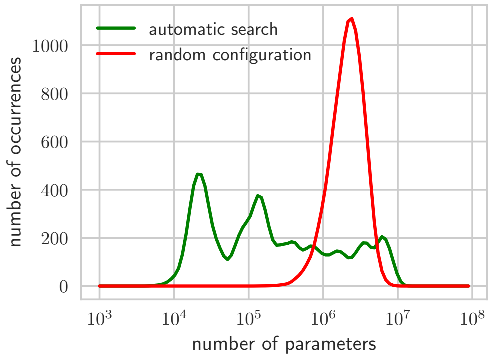

(d) Automatic law on S_2

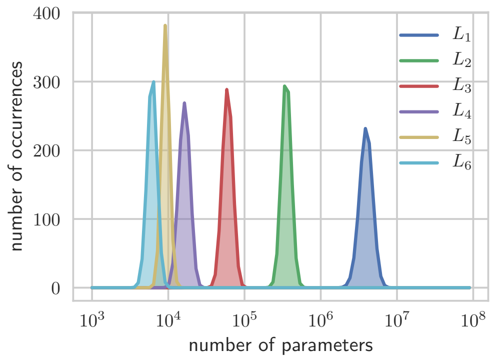

(e) Manual laws on S_3

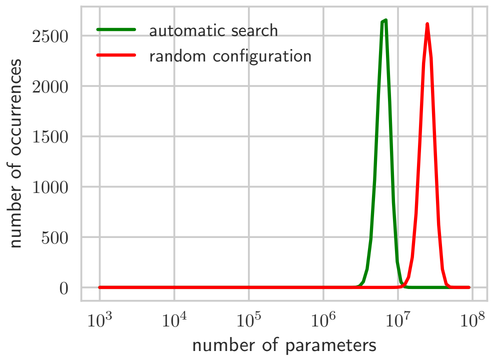

(f) Automatic law on S_3

are obtained by uniformly sampling each parameter in its full domain (according to the law L_0 in the previous tables) and when they are obtained with automatically generated sampling laws that are adjusted with our proposed genetic algorithm. The base law of the original definition has a high impact on where the actual mass of the distribution concentrates. The main densities are around 10^6 parameters for S_1 and S_2. S_3 and S_4 have the center of mass above 10^7 parameters which cause difficulties for the genetic algorithm to converge towards the low end of the domain. Still, in all cases, the genetic algorithm is capable of either considerably moves the center of mass to the left or to flatten out the distribution. For completeness, Table 7 states the parameter and flop metrics obtained with our defined search spaces.

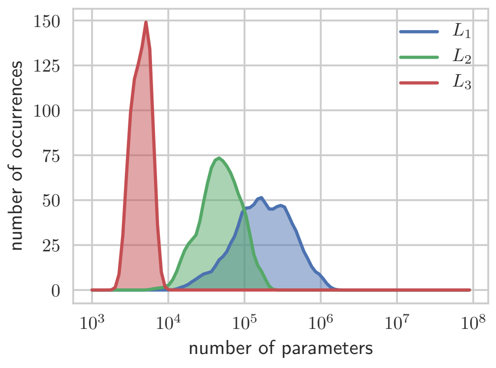

(g) Manual laws on S_4

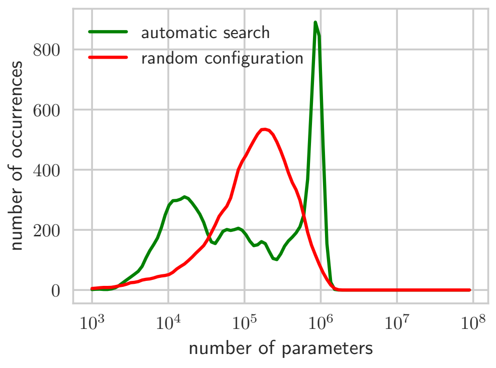

(h) Automatic law on S_4

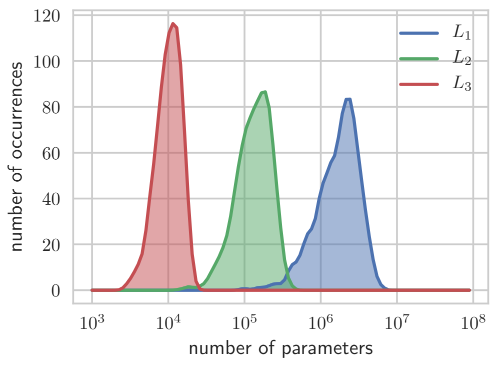

(i) Manual laws on S_5

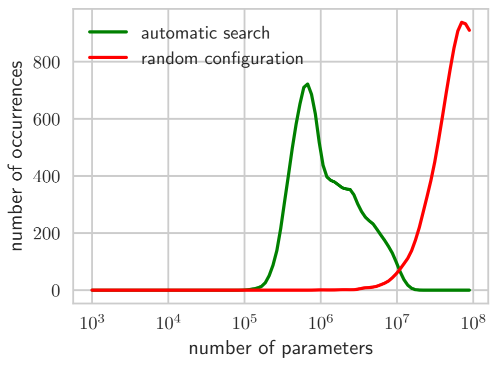

(j) Automatic law on S_5

Figure 1: Statistic over manual (left) and automatic generated (right) networks for all search spaces S_1 up to S_5. With manually design the sampling law, a human expert can reasonably adjust and focus the distribution into regions of interest, either close to a target constraint and in a general way to cover five orders of magnitude.

3 Training setup

We conducted all training experiments in a controlled environment where we trained from scratch for each candidate architecture. We used PyTorch version 0.4.1 as development framework and run on IBM Power8 or Power9 nodes equipped with either P100 or V100 GPUs. We used standard on-the-fly data augmentation during training that pads images with 4 pixels and randomly crops the image to 32×32 pixels, apply horizontal flipping with a probability of 0.5 and finally normalizes pixel values to zero mean and unit variance. During testing, the original 32×32 images are directly normalized and feed into the models. For training, we used stochastic gradient descent with a batch size of 128 samples configured with an initial learning rate of 0.01, a momentum of 0.9, and a weight decay factor of $5 * 10^{-4}$. We used a fixed scheduling schema where the learning rate is divided by a factor of 10 at epoch 40 and 70 and we limit training to stop at 100 epochs.

4 Deployment setup

In our work, we decided to demonstrate our algorithm to produce optimized network architectures for the Raspberry-Pi 3(B+) as stated in our paper. At this point, we consider it worth to justify our choice. First, it should be mentioned that there is a current emerging trend in industry and research that pushes to improve hardware for artificial intelligence (AI) by either improving performance, reducing power consumption or providing better trade-offs in terms of power/performance ratios or hardware cost versus the on-device supported features. In terms of thinking through IoT driven business cases, the fact that new hardware appears requires to benchmark and rethink on what HW

Table 7: Overview of parameters and flop metrics of generated architecture search spaces. We started from seven well-known topologies and defined at least three sampling laws per narrow search. The generated search spaces cover over three order of magnitudes in the amount of weights and flops.

Search space		Number of parameters			Number of flops		
		Min	Mean+/-Std	Max	Min	Mean+/-Std	Max
DenseNet	L1	5.8e+2	2.6e+4+/-2.3e+4	1.2e+5	1.5e+5	7.5e+6+/-7.2e+6	3.3e+7
	L2	0.e+0	2.3e+5+/-2.3e+5	1.6e+6	0.e+0	6.9e+7+/-7.6e+7	4.0e+8
	L3	5.6e+3	2.8e+6+/-3.e+6	1.9e+7	4.5e+5	7.6e+8+/-9.1e+8	4.8e+9
MobileNetV2	L1	9.5e+2	1.6e+3+/-2.0e+2	2.2e+3	1.8e+5	4.5e+5+/-1.7e+5	1.2e+6
	L2	2.5e+3	5.4e+3+/-1.4e+3	9.6e+3	9.e+5	2.8e+6+/-1.2e+6	6.6e+6
	L3	8.8e+3	2.0e+4+/-5.1e+3	4.0e+4	1.4e+6	5.9e+6+/-3.2e+6	2.1e+7
	L4	2.8e+4	6.9e+4+/-1.6e+4	1.3e+5	2.2e+6	1.5e+7+/-1.1e+7	7.2e+7
	L5	1.2e+5	4.3e+5+/-1.5e+5	9.9e+5	8.6e+6	1.0e+8+/-8.4e+7	6.9e+8
	L6	3.1e+5	2.7e+6+/-1.2e+6	7.8e+6	2.1e+7	6.3e+8+/-5.7e+8	4.0e+9
GoogLeNet	L1	4.5e+3	6.5e+3+/-5.4e+2	8.3e+3	1.8e+6	2.6e+6+/-2.8e+5	3.4e+6
	L2	8.8e+3	9.8e+3+/-3.2e+2	1.1e+4	3.3e+6	3.8e+6+/-1.9e+5	4.3e+6
	L3	1.3e+4	1.7e+4+/-2.e+3	2.2e+4	4.9e+6	8.7e+6+/-1.9e+6	1.3e+7
	L4	4.5e+4	6.4e+4+/-6.3e+3	8.0e+4	1.6e+7	2.9e+7+/-5.7e+6	4.3e+7
	L5	2.8e+5	3.8e+5+/-3.2e+4	4.9e+5	1.0e+8	1.5e+8+/-1.9e+7	2.1e+8
	L6	2.4e+6	4.2e+6+/-6.6e+5	6.8e+6	8.0e+8	1.5e+9+/-3.1e+8	2.5e+9
PNASNet	L1	2.7e+3	4.8e+3+/-1.2e+3	7.6e+3	9.4e+5	1.8e+6+/-4.9e+5	2.8e+6
	L2	6.8e+3	6.0e+4+/-3.6e+4	2.1e+5	2.4e+6	1.6e+7+/-8.e+6	4.4e+7
	L3	1.6e+4	2.6e+5+/-2.2e+5	1.5e+6	4.1e+6	5.1e+7+/-3.3e+7	2.e+8
ResNeXt	L1	3.0e+3	1.1e+4+/-3.9e+3	2.2e+4	1.6e+6	6.1e+6+/-2.6e+6	1.2e+7
	L2	1.5e+4	1.6e+5+/-7.4e+4	4.5e+5	3.7e+6	7.e+7+/-4.e+7	2.1e+8
	L3	1.0e+5	2.1e+6+/-1.1e+6	6.8e+6	2.1e+7	8.5e+8+/-5.8e+8	2.7e+9

product a certain IoT application should be built. We are aware of the existence of tens of ASIC or FPGA solutions that might be selected for business legitimated reasons as a target edge inference system.

We think that the crucial factors for a successful IoT deployment strategy cover the following points with an importance that is application specific:

- reliability
- user/developer friendly software ecosystem
- modular integration or extensions of different functionality
- typical IoT support
- cost efficient system

We decided that in this work we focus on the algorithm. However, since we are aware of many choices and good reasons for a certain HW solution, we developed our approach such that the main functionality is decoupled from the actual HW implementation. Especially, populating a database with the current results that are obtained with expensive training for obtaining the model accuracy, can easily be reused later on for any hardware platform by just implementing the inference and timing measurement setup in order to obtain the new HW calibration information. In this work, we focus on the most general use-case that causes the least amount of requirements for the underlying hardware. That way, we identified the Raspberry-Pi 3(B+) as general purpose quad-core architecture as a suitable IoT device candidate. The Raspberry-Pi proves its marketability by the fact that it has been shipped over 25 million times by February 2019 [4]. Even though there are competing products that are specially tailored for AI deployment, the choice of selecting a general-purpose platform equipped with a Linux operating system comes with obvious advantages, such that it enables to reuse established software and solutions can be easily extended to any needs. In contrast to dedicated AI accelerators that are shipped as USB dongles, potentially required features such as Ethernet, WiFi, SDCard slot, or USB ports are already included in the Raspberry-Pi 3(B+). Even though we are aware that a general purpose architecture cannot compete in some performance metrics with a dedicated AI product, we argue that our work is especially insightful since we cover the more challenging case on optimizing for a performance limited device. In our view, it is plausible enough to argue that a more performant device will automatically deliver better results. We aim to support various HW platforms with different deployment flows in future work.

Next, we describe the deployment flow for the Raspberry-Pi 3(B+). Even though our back-end algorithms, as well as our training routine, is implemented in PyTorch, we still aim to remove the back-end dependency in order to be open and to ease later migration to new target platforms, frameworks, and ecosystems. To that end, we decided to export all models according to the open neural network exchange (ONNX) format [2]. We decided to use caffe2 as target device runtime for the exported ONNX models. We build the caffe2 framework directly from a full source compilation with all default parameters on the Raspberry-Pi 3(B+) and we ensured that the produced code is using the ARMs NEON library [1] for fast computation. We wrote a light script to import the produce ONNX models and we trigger a sequence of inferences for a single image. In our work, all timing results have been obtained by averaging wall clock times over ten runs.

5 Datasets

Our large-scale search that provides Pareto optimal fronts is conducted on CIFAR10 [14] with the provided train and test splitting. We demonstrate the scalability of our architecture search by applying a fast customized search to individual datasets. In contrast to previous architecture searches that include training inside the main optimization loop, we can sample a very large amount of neural networks in a short time *without* training. Additionally, we can run the genetic algorithm to bias the sampling process into domains we are interested *without* any single network training step. With our approach, customized searches become affordable. For each dataset we performed the following workflow: we define an upper constraint τ, we run a genetic search with the optimization goal to deliver a sampling law with a probability density function that is concentrated in $\tau_1 = 0.5\tau, \tau_2 = \tau$, we sample 100 candidate networks from the found sampling law, we filter out the good models that strictly satisfy the one-sided constraint $< \tau$ and we randomly select 10 suitable networks. Finally, only 10 candidate networks are entering the compute-intensive trained procedure. This approach allows affording to validate our algorithm on thirteen datasets for three considered constraints. Figure 8 of our paper presents the results. The following explains the considered datasets.

We focus on sixteen public available and established image classification datasets: *MNIST* [9], *GTSRB* [19], *svhn* [16], *CIFAR10* [14], *flowers*[1], *flowers102* [17], *fashion MNIST* [21], *food101* [6], *CIFAR100* [14], *stl10* [8], *textures* [7], *indoor67* [18], *caltech256* [10], *quickdraw*[2], and *places* [23]. Figure 2 shows the number of classes, Figure 3 shows the balance of the classes as ratio of samples of the majority over the minority class, and Figure 4 shows the number of samples used for training and testing. The datasets span two order of magnitudes in the number of classes and in the number of available training samples and one order of magnitude in the balance ratio. The datasets stem from various domains and cover typical and relevant use cases such as optical digit recognition stemming from handwritten samples (*MNIST*) or in the context of images stemming from house numbers (*svhn*). *GTSRB* covers traffic sign recognition, a use case that occurs in autonomous driving systems. Scene recognition aims to classify the location of where the picture was taken as whole (*indoor67* and *places*), whereas traditional classification tasks are posed around identifying a class based on a particular object present within the image. In order to limit the workload, we run our proposed algorithm on 13 out of 16 datasets that have less than 100'000 images in the training set. Results are presented in Figure 8 of our paper.

[1]Available at `http://download.tensorflow.org/example_images/flower_photos.tgz`

[2]Available at `https://github.com/googlecreativelab/quickdraw-dataset`

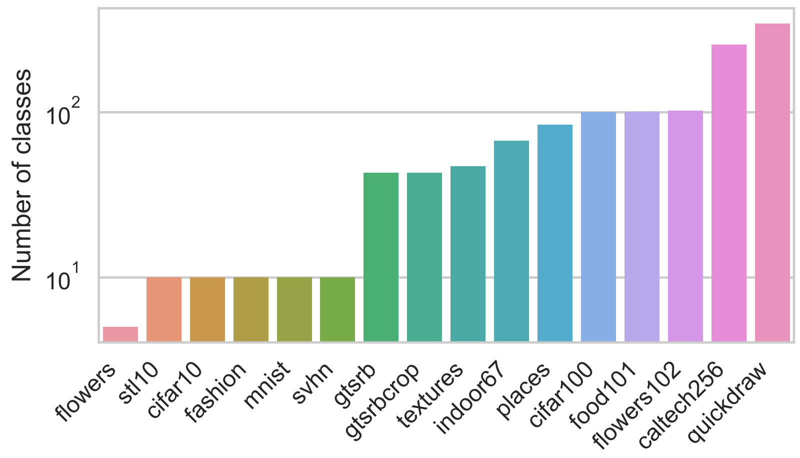

Figure 2: The number of classes per dataset cover two orders of magnitude, from as few as 5 classes up to 345 classes.

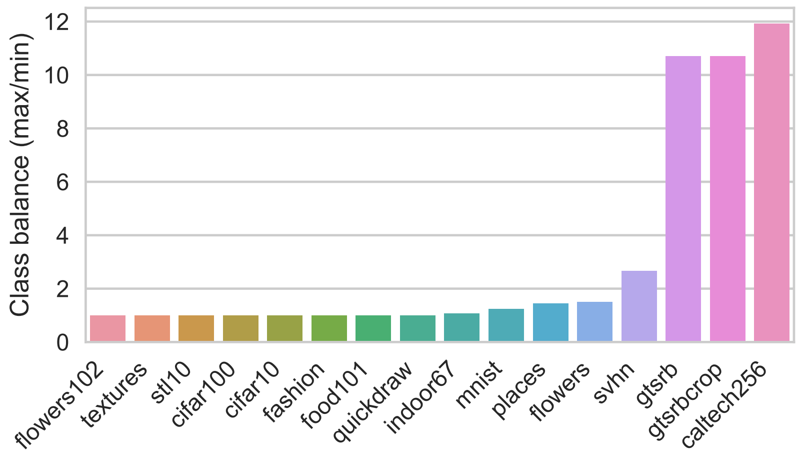

Figure 3: Ratio of class samples of majority over minority class in the training data. The balance ratio spans from 1.0 (for equally balanced datasets) up to a factor of 11.9×.

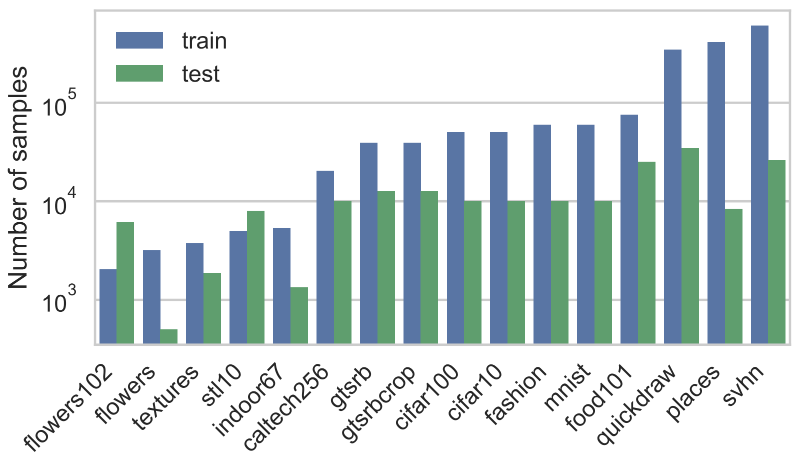

Figure 4: The number of samples within a given dataset used for training and testing sorted by training samples. Train and test sets are always disjoint and the splitting is given as suggested by the reference. The number of training samples spans more than two order of magnitude.

References

[1] Arm neon. `https://www.arm.com/why-arm/technologies/neon`. Accessed: 2019-05-22.

[2] Onnx: Open neural network exchange format. `https://onnx.ai/`. Accessed: 2019-05-22.

[3] Pytorch. `https://pytorch.org/`. Accessed: 2019-05-22.

[4] Raspberry pi celebrates 25 millionth sale as 7th anniversary arrives. `https://www.tomshardware.com/news/raspberry-pi-25-million-sold,38724.html`. Accessed: 2019-05-22.

[5] Train cifar10 with pytorch. `https://github.com/kuangliu/pytorch-cifar`. Accessed: 2019-05-22.

[6] L. Bossard, M. Guillaumin, and L. Van Gool. Food-101 – mining discriminative components with random forests. In D. Fleet, T. Pajdla, B. Schiele, and T. Tuytelaars, editors, *Computer Vision – ECCV 2014*, pages 446–461, Cham, 2014. Springer International Publishing.

[7] M. Cimpoi, S. Maji, I. Kokkinos, S. Mohamed, and A. Vedaldi. Describing textures in the wild. In *Proceedings of the 2014 IEEE Conference on Computer Vision and Pattern Recognition*, CVPR '14, pages 3606–3613, Washington, DC, USA, 2014. IEEE Computer Society.

[8] A. Coates, A. Ng, and H. Lee. An analysis of single-layer networks in unsupervised feature learning. In G. Gordon, D. Dunson, and M. Dudík, editors, *Proceedings of the Fourteenth International Conference on Artificial Intelligence and Statistics*, volume 15 of *Proceedings of Machine Learning Research*, pages 215–223, Fort Lauderdale, FL, USA, 11–13 Apr 2011. PMLR.

[9] L. Deng. The mnist database of handwritten digit images for machine learning research [best of the web]. *IEEE Signal Processing Magazine*, 29(6):141–142, 2012.

[10] G. Griffin, A. Holub, and P. Perona. Caltech-256 object category dataset. 2007.

[11] K. He, X. Zhang, S. Ren, and J. Sun. Deep residual learning for image recognition. In *The IEEE Conference on Computer Vision and Pattern Recognition (CVPR)*, June 2016.

[12] A. G. Howard, M. Zhu, B. Chen, D. Kalenichenko, W. Wang, T. Weyand, M. Andreetto, and H. Adam. Mobilenets: Efficient convolutional neural networks for mobile vision applications. *CoRR*, abs/1704.04861, 2017.

[13] G. Huang, Z. Liu, L. van der Maaten, and K. Q. Weinberger. Densely connected convolutional networks. In *The IEEE Conference on Computer Vision and Pattern Recognition (CVPR)*, July 2017.

[14] A. Krizhevsky and G. Hinton. Learning multiple layers of features from tiny images. 2009.

[15] C. Liu, B. Zoph, M. Neumann, J. Shlens, W. Hua, L.-J. Li, L. Fei-Fei, A. Yuille, J. Huang, and K. Murphy. Progressive neural architecture search. In *The European Conference on Computer Vision (ECCV)*, September 2018.

[16] Y. Netzer, T. Wang, A. Coates, A. Bissacco, B. Wu, and A. Y. Ng. Reading digits in natural images with unsupervised feature learning. In *NIPS workshop on deep learning and unsupervised feature learning*, volume 2011, page 5, 2011.

[17] M. E. Nilsback and A. Zisserman. Automated flower classification over a large number of classes. In *2008 Sixth Indian Conference on Computer Vision, Graphics Image Processing*, pages 722–729, Dec 2008.

[18] A. Quattoni and A. Torralba. Recognizing indoor scenes. In *2009 IEEE Conference on Computer Vision and Pattern Recognition*, pages 413–420, June 2009.

[19] J. Stallkamp, M. Schlipsing, J. Salmen, and C. Igel. The german traffic sign recognition benchmark: A multi-class classification competition. In *The 2011 International Joint Conference on Neural Networks*, pages 1453–1460, July 2011.

[20] C. Szegedy, V. Vanhoucke, S. Ioffe, J. Shlens, and Z. Wojna. Rethinking the inception architecture for computer vision. In *The IEEE Conference on Computer Vision and Pattern Recognition (CVPR)*, June 2016.

[21] H. Xiao, K. Rasul, and R. Vollgraf. Fashion-mnist: a novel image dataset for benchmarking machine learning algorithms, 2017.

[22] S. Xie, R. Girshick, P. Dollar, Z. Tu, and K. He. Aggregated residual transformations for deep neural networks. In *The IEEE Conference on Computer Vision and Pattern Recognition (CVPR)*, July 2017.

[23] B. Zhou, A. Lapedriza, A. Khosla, A. Oliva, and A. Torralba. Places: A 10 million image database for scene recognition. *IEEE Transactions on Pattern Analysis and Machine Intelligence*, 2017.